

Mechanistic investigation on the toxicity of MgO nanoparticles toward cancer cells†Karthikeyan Krishnamoorthy,^a Jeong Yong Moon,^b Ho Bong Hyun,^b Somi Kim Cho^{*b} and Sang-Jae Kim^{*ac}

Received 31st July 2012, Accepted 20th September 2012

DOI: 10.1039/c2jm35087d

Magnesium oxide nanoparticles (MgO NPs) are increasingly recognized for their applications in cancer therapy such as nano-cryosurgery and hyperthermia. The present study investigated the cytotoxic effects of magnesium oxide nanoparticles (MgO NPs) against normal lung fibroblast cells and different types of cancerous cells. MgO NPs exhibited a preferential ability to kill cancerous cells such as HeLa, AGS and SNU-16 cells. A detailed study has been undertaken to investigate the mechanism of cell death occurring in cancer cells (AGS cells) by the analysis of morphological changes, western blot analysis and flow cytometry measurements. Western blot analysis measurements suggested the role of apoptosis in cell death due to MgO exposure. MgO NPs enhanced ultrasound-induced lipid peroxidation in the liposomal membrane. Flow cytometry measurements using H₂DCFDA showed that the toxicity of MgO NPs is attributed to the generation of reactive oxygen species, which further results in the induction of apoptosis in cancer cells. Our experimental results suggested the potential utility of MgO NPs in the treatment of cancer.

Introduction

Cancer is one of the leading diseases throughout the world in which a group of cells display uncontrolled growth, invasion, and sometimes metastasis.¹ According to the American Cancer Society, more than 11 000 women develop cervical cancer each year in the United States, and about 4000 die from the disease (ACS, 2009).² The present treatments in cancer therapy, including surgery, radiation, photodynamic therapy and conventional chemotherapy, have severe limitations, for example they can affect all the cells in the body.^{3,4} In this regard, nano-sized particles with their size comparable to that of biological structures are very smart materials for the manipulation, sensing, and detection of biological systems.^{5,6} Recent progress in utilizing inorganic nanoparticles for biomedical applications has received more attention due to their pronounced applications as potential antibacterial agents, drug and gene delivery vehicles, and in molecular diagnostics and cancer therapy.^{7–9} The toxicity of nanoparticles towards diseased cells would create a new criterion for the development of their potential applications in

the field of medicine.¹⁰ Our previous report showed that ZnO NPs possess toxicity towards cancer cells.⁷ There are evidential reports available in the literature demonstrating the antimicrobial and anticancer activities of silver, gold, ZnO and TiO₂ nanoparticles.^{11–14} Surface modified gold nanorods are used for fast and selective cancer cell uptake and also as contrast agents for multimodal imaging of cancer.^{12,15} Ahamed *et al.* investigated the role of oxidative stress in the toxicity of ZnO nanorods towards human alveolar adenocarcinoma cells.¹³ Similarly, there are reports showing that surface engineered nanoparticles such as hydroxyl/amine functionalized TiO₂ nanoparticles can be used to eradicate cancer cells.¹⁴ There is always a demand for creating and exploring new novel materials for biological applications especially in the field of medicine owing to their huge impact on health care.

MgO nanoparticles are well known for their biological applications as an antibacterial agent, for the relief of heartburn and bone regeneration.¹⁶ MgO is one of the six magnesium compounds which are currently recognized as safe by the U.S. Food and Drug Administration (21CFR184.1431). Magnesium salt has been used for the treatment of magnesium deficiency. Stoimenov *et al.* demonstrated that MgO nanoparticles and their halogenated adducts exhibit strong antibacterial activity through membrane disruption.¹⁷ Previous reports show that the considerable antibacterial activity of MgO is attributed to the generation of reactive oxygen species (ROS) on the oxide surface.^{18,19} Even though MgO NPs serve as a potential antibacterial agent and are used in several biological applications, their toxicity towards cancer cells remains an undeveloped area. Considering the efforts taken until now on the cellular activity and medicinal

^aNanomaterials and System Laboratory, Department of Mechanical Engineering, Jeju National University, Jeju – 690 756, Republic of Korea. E-mail: kimsangj@jeju.ac.kr

^bFaculty of Biotechnology, College of Applied Life Sciences, Jeju National University, Jeju – 690 756, Republic of Korea. E-mail: phd.kim.somi@gmail.com

^cNanomaterials and System Laboratory, Department of Mechatronics Engineering, Jeju National University, Jeju – 690 756, Republic of Korea

† Electronic supplementary information (ESI) available. See DOI: 10.1039/c2jm35087d

applications of MgO nanoparticles, there are only limited reports available in the literature. Ge *et al.* reported the cytotoxicity of MgO NPs towards human umbilical vein endothelial cells.²⁰ Sun *et al.* examined the cytotoxicity of several metal oxide nanoparticles including MgO NPs on human cardiac microvascular endothelial cells.²¹ Lai *et al.* reported that MgO NPs possess less cytotoxic effects against human astrocytoma U87 cells when compared to ZnO and TiO₂ NPs.²² Boubeta *et al.* reported the application of Fe/MgO nanoshells as an MRI agent in cancer therapy.²³ Chalkidou *et al.* demonstrated the application of Fe/MgO nanoparticles as a magnetically mediated hyperthermia agent in cancer therapy.²⁴ An MgO based magnetic tunnel junction sensor together with magnetic nanoparticles is used as biosensors for liver cancer immunoassay.²⁵ More recently, Di *et al.* reported the promising application of MgO NPs in nanocryosurgery for tumor treatment.²⁶ Hence, the toxicity of MgO NPs towards cancer cells remains an area of potential interest. The purpose of this study is to explore the toxicity of MgO nanoparticles against cancer cells and their mechanistic investigation on cell death.

Experimental methods

Materials used

Magnesium nitrate and sodium hydroxide were obtained from Dae Jung chemicals, South Korea. All the chemicals obtained are of research grade that can be used without further purification.

Preparation of MgO NPs

MgO NPs were prepared by the precipitation method using magnesium nitrate and sodium hydroxide (NaOH) as precursors.²⁷ Briefly, 0.2 M solution of NaOH was slowly added dropwise into a 0.1 M solution of magnesium nitrate in 50 ml of water with vigorous stirring for 2 h. The white precipitate formed containing Mg(OH)₂ was washed thoroughly with distilled water and centrifuged at 4000 rpm for 15 minutes. The procedure was repeated several times until the precipitate was free from any trace of impurities. The precipitate was dried at 100 °C followed by calcination at 400 °C resulting in the formation of MgO NPs.

Characterization of MgO NPs

The phase purity and crystallinity of the MgO NPs were determined by X-ray diffraction (XRD) recorded on a X-ray diffractometer system (D/MAX 2200H, Bede 200, Rigaku Instruments C). High resolution transmission electron microscopy (HR-TEM) measurement and the SAED pattern were studied using a HR-TEM, FEI Titan 80-300 instrument. The hydrodynamic particle size of the MgO NPs was measured on a ZetaSizer (Nano-Z, Malvern Instruments Ltd, UK). The UV-vis spectra were recorded using a spectrophotometer (Shimadzu UV-315, Japan). Fourier transform infrared (FTIR) spectra were measured at room temperature with an FTIR spectrometer (Thermo Scientific Systems, Nicolet-6700) using the KBr pellet technique. Raman spectra of the MgO NPs were studied using a LabRam HR800 micro-Raman spectroscope (Horiba Jobin-

Yvon, France). The Raman system was operated at a 10 mV laser power and an excitation wavelength of 514 nm with an Ar⁺ ion laser. The photoluminescence spectrum was measured using a spectrofluorophotometer (Shimadzu instruments – RF5301 model).

Reagents used

Fetal bovine serum (FBS), RPMI, DMEM, and H₂DCFDA were purchased from Invitrogen, USA. Hoechst 33342, 3-(4,5-dimethylthiazol-2-yl)-2,5-diphenyltetrazolium bromide (MTT) and dimethyl sulfoxide (DMSO) were purchased from Sigma Chemical Co. (St Louis, MO). Cleaved PARP, Bcl-2, and β-actin antibodies were purchased from Cell Signaling (Danvers, MA). Polyvinylidene fluoride (PVDF) membranes for Western blotting were purchased from Millipore (Billerica, MA). The chemicals used for lipid peroxidation measurement such as ferric chloride (FeCl₃), L-ascorbic acid, trichloroacetic acid (TCA) and thio-barbituric acid (TBA) were purchased from Sigma-Aldrich, South Korea.

Cell cultures

Cancer cell lines, including HeLa, a human cervix adenocarcinoma cell line, AGS, a human gastric adenocarcinoma cell line, SNU-16, a human gastric carcinoma cell line, and CCD-25Lu, a human lung fibroblast cell line (normal cells), were obtained from the Korean Cell Line Bank (Seoul, Korea). The cell lines were cultured in DMEM or RPMI 1640 containing 10% (v/v) heat-inactivated FBS, 100 units per ml penicillin, and 100 μg ml⁻¹ streptomycin. Cells were maintained in a humidified incubator at 37 °C in a 5% CO₂ atmosphere.

Cell viability assay

The effect of MgO NPs on the cell viability was determined by a 3-(4,5-dimethylthiazol-2-yl)-2,5-diphenyl-tetrazolium bromide (MTT) assay, which is based on the conversion of MTT to formazan crystals by mitochondrial dehydrogenases.^{28,29} Briefly, HeLa cells (4 × 10³ cells per well), AGS, SNU-16 and CCD-25Lu cells (1 × 10⁴ cells per well) were seeded in 96-well culture plates. After overnight incubation, cells were treated with various concentrations of MgO NPs for 24, 48 and 72 h. Then, 0.1 mg of MTT was added to each well, and the cells were incubated at 37 °C for 4 h. The medium was removed, and then 150 μl of DMSO was added to each well to dissolve the formazan crystals. Absorbance was read at 570 nm on a microplate reader (Tecan, Salzburg, Austria).

Analysis of morphological changes

Hoechst 33342 staining experiments³⁰ were performed in order to study the apoptotic behavior and the morphological changes of cells after exposure to MgO NPs. Briefly, the AGS cells were treated with MgO NPs for 24 and 48 h. After the exposure time, 10 μM of Hoechst 33342, a DNA-specific fluorescent dye, was added to the solution in each well and the plates were incubated for 10 min at 37 °C. The stained cells were then observed under an Olympus fluorescence microscope.

Western blot analysis

After treatment, the cells were collected and washed twice with cold PBS. The cells were then lysed in lysis buffer (100 mM Tris-HCl, pH 8, 250 mM NaCl, 0.5% Nonidet P-40, 1× cocktail of protease inhibitor), disrupted by sonication and extracted at 4 °C for 30 min. The lysates were then centrifuged at 13 000× rpm at 4 °C for 25 min. The protein concentration was determined by the BCA™ Protein Assay (Pierce, Rockford, IL, USA). Aliquots of the lysates were separated by 12–15% SDS-PAGE and transferred onto the PVDF membrane. After blocking with 5% non-fat dried milk, the membrane was incubated for 2 h with primary antibodies, followed by 30 min with secondary antibodies. Human anti-cleaved PARP, -caspase-3, -Bcl-2 (diluted 1 : 1000) and anti-β-actin antibodies (1 : 10 000) were used as the primary antibodies with horseradish peroxidase (HRP)-conjugated goat anti-rabbit IgG (Vector Laboratories, USA) and HRP-conjugated goat anti-mouse IgG (Invitrogen, USA) (both 1 : 5000) as secondary antibodies. Protein bands were detected using the WEST-ZOL® plus Western Blot Detection System (iNtRON, Gyeonggi-do, Korea).³¹

Flow cytometric analysis of ROS production

AGS cells (4×10^4 cells per ml) were seeded in 60 mm dishes and treated with MgO ($300 \mu\text{g ml}^{-1}$) for 6 h. The cells were incubated with H₂DCFDA for 30 min at 37 °C. Next, the cells were harvested and washed with PBS. All analyses were performed using a FACS Caliber flow cytometer (BD Biosciences). Data from 10 000 cells per sample were analyzed with Cell Quest Software (BD Biosciences).

Lipid peroxidation measurement

The effect of reactive oxygen species/free-radical modulation activity of MgO NPs was also examined using a lipid peroxidation assay.⁷ Herein, lipid peroxidation was induced in liposomes prepared by ultrasonic irradiation from egg lecithin by adding 5 μl of 200 mM L-ascorbic acid and 5 μl of 400 mM FeCl₃. To this, appropriate concentrations of MgO NPs were added. A control containing no compound was prepared. The samples were incubated at 37 °C for 1 h. The reaction was inhibited by adding 1 ml of stopping solution containing 0.25 M HCl, 1.5% (vol/vol) TCA, and 0.375% (wt/vol) TBA. These reaction

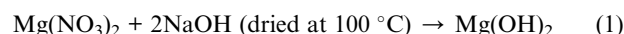
mixtures were kept in a boiling-water bath for 15 min, cooled, and centrifuged. The absorbance of the resulting solution was measured at 532 nm.

Statistical analysis

All presented data were repeated at least three times. Values are expressed as means ± S.D. of triplicate. Statistical analysis was performed using analysis of variance (ANOVA). Values of **P* < 0.05 were considered to be statistically significant.

Results and discussion

In this study, MgO NPs were prepared by the precipitation method using magnesium nitrate and sodium hydroxide (NaOH) as precursors.²⁷ Briefly, aqueous solutions of Mg(NO₃)₂ and NaOH were mixed at 25–30 °C, and a precipitation reaction occurred between the Mg⁺ ions and OH⁻ ions during stirring for 2 hours which results in the formation of magnesium hydroxide.



Furthermore, the resulting hydroxide precipitate was calcined at 400 °C, which led to the decomposition of Mg(OH)₂ to MgO NPs.



Fig. 1(a) shows the XRD pattern of MgO NPs synthesized by the precipitation method, confirming the presence of the cubic MgO phase. The peaks at $2\theta = 36.88^\circ$, 49.28° and 62.22° were assigned to (011), (200) and (220) planes of cubic MgO nanoparticles. The diffraction peaks matched well with the standard diffraction pattern of MgO (JCPDS 45-0946). No characteristic peaks of impurities were detected suggesting that high purity MgO was obtained. The average crystallite size calculated from the Debye Scherer equation³² was 20 nm. Fig. 1(b) represents the HR-TEM image of the MgO NPs, which depicts the presence of nanosized particles with some of the particles interconnected with each other. The inset of Fig. 1(b) shows the selected area diffraction (SAED) pattern of MgO NPs, which confirms the nanocrystalline nature and can be indexed to the cubic phase MgO NPs.³³ The SAED pattern of the synthesized MgO NPs is in agreement with the XRD pattern and also with the previously

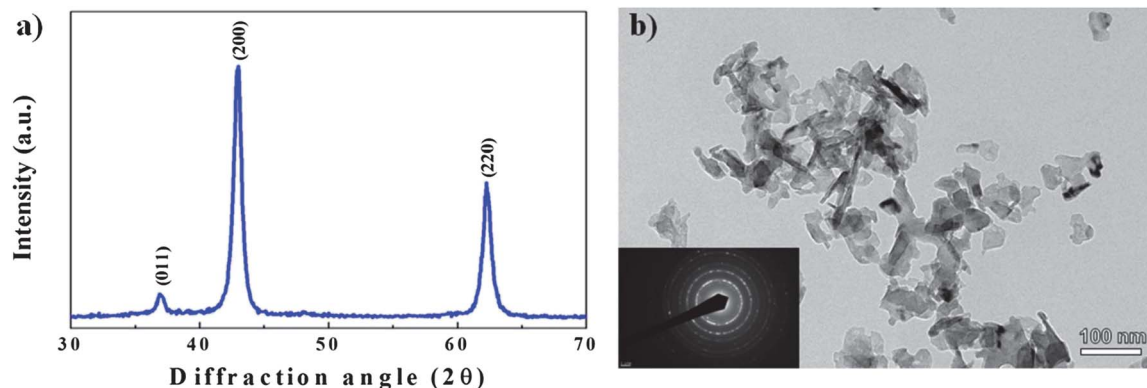


Fig. 1 (a) X-ray diffraction pattern of MgO nanoparticles. (b) HR-TEM image of MgO nanoparticles and their corresponding SAED pattern.

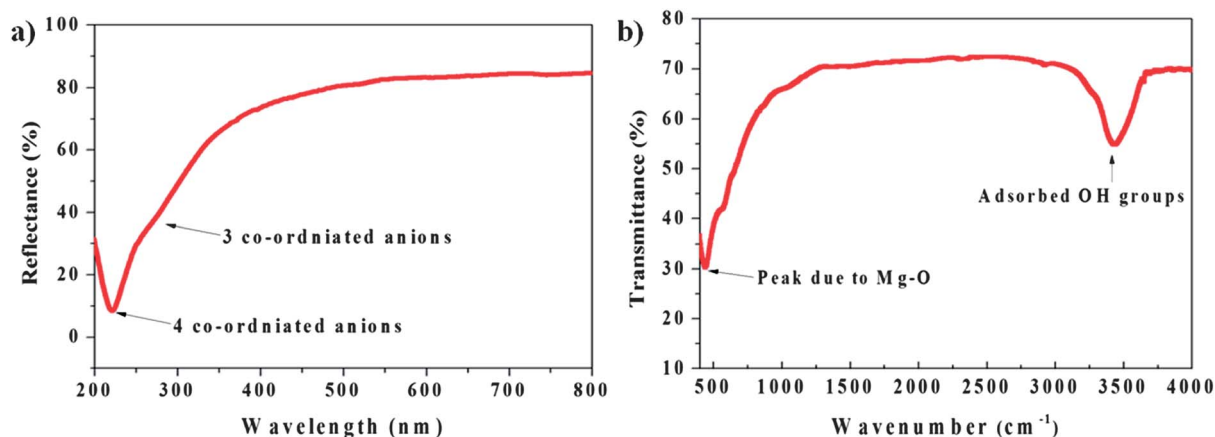


Fig. 2 (a) UV-vis diffuse reflectance spectrum of MgO nanoparticles. (b) FT-IR spectrum of MgO nanoparticles.

published report.³⁰ Fig. 2(a) shows the UV-vis diffuse reflectance spectrum of MgO nanoparticles. The reflection minima were found at 221 nm and 270 nm, which can be attributed to the electronic excitations of 4-coordinated surface anions at the edges and 3-coordinated surface anions at the corners.³⁴ The optical band gap value calculated from the UV-vis spectra was 5.6 eV, which is in good agreement with a previously published report.³⁵ The lower band gap of MgO NPs is due to the presence of 4-coordinated surface anions at the edges in the MgO NPs whereas the bulk material possesses a band gap of 7.8 eV due to the presence of 6-coordinated surface anions. This is in agreement with the previous study of Berger *et al.*³⁶ Fig. 2(b) shows the FTIR spectrum of MgO NPs. It shows a strong band at 442 cm^{-1} which corresponds to the stretching vibration of MgO.³⁷ The broad band around 3400 cm^{-1} indicates the presence of adsorbed OH groups on the MgO surface.³⁷ Furthermore, the crystalline nature of the synthesized MgO NPs was studied using the Raman spectroscopic analysis. Fig. 3 shows the typical Raman spectrum of MgO NPs, which shows the presence of two characteristic bands at 290 and 446 cm^{-1} . The former is associated with a TA phonon at the zone boundary whereas the latter is associated with a TA phonon at the zone center. The observed Raman lines are closely matched with the previous results of Kim *et al.* and Ishikawa *et al.*^{38,39} Moreover, the observed bands in the Raman

spectrum confirm the presence of the nanocrystalline phase since these bands are generally absent in the bulk MgO.³⁹

Defects or oxygen vacancies in the metal oxide surface act as an invisible agent and have a significant role in the optical, electronic and biological properties.⁴⁰ In these aspects, studying the presence of defects or oxygen vacancies in the MgO surface is highly important. Being a wide-band gap material, MgO generally does not exhibit photoluminescence. However, the charge transfer on the surface state may result in luminescence as reported by Xie *et al.*⁴¹ Hence, we measured the photoluminescence spectrum of MgO NPs, which is shown in Fig. 3(b). It shows the presence of a strong peak positioned around 450 nm which is not due to the band gap emission. The occurrence of PL emission in the MgO NPs is due to the presence of defects/oxygen vacancies on the metal oxide surface.⁴² Similarly, a previous study on the photoluminescence of MgO nano-disks showed emission around 420 nm, which was attributed to the presence of oxygen vacancies.³⁵ The presence of oxygen vacancies on the surface of MgO NPs is due to the synthesis process during which the transformation of $\text{Mg}(\text{OH})_2$ into MgO NPs results in incomplete oxidation which may give emission. This is consistent with the previous studies of Kumari *et al.* and Hao *et al.*^{35,42,43} Overall, the presence of oxygen vacancies on the MgO surface is confirmed by the photoluminescence study.

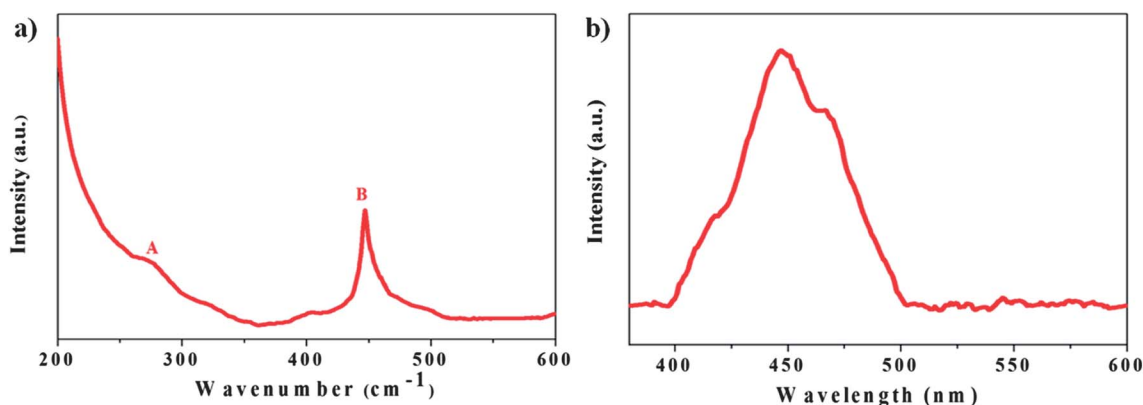


Fig. 3 (a) Raman spectrum of MgO nanoparticles. (b) Photoluminescence spectrum of MgO nanoparticles.

The stability of nanoparticles in the dispersion state is one of the significant issues to be examined prior to their biological applications.⁴⁴ Hence, we employed the DLS technique to measure the particle size and the size distribution of MgO NPs in aqueous dispersion. The DLS measurements of MgO NPs are given in the ESI (Fig. S1†) which shows that the average hydrodynamic size of the MgO NPs is about 137 nm and is comparatively larger than the observed particle size from XRD and TEM. The higher size obtained from DLS measurements is mainly due to the fact that DLS measures the hydrodynamic size as an ensemble collection of particles in solution.^{45,46} This finding is supported by previous results of other investigators for the DLS measurement of metal oxide nanoparticles.^{47,48} This study suggested that the MgO NPs possess a good stability in solution.

The use of MgO NPs in biological applications as antibacterial agents, magnetic hyperthermia agents, MRI contrast agents and in nano-cryosurgery is already reported in the literature.^{19,23,24,26} In these aspects, a study on the mechanistic toxicity of MgO NPs against cancer cells will reveal some special features of this material. Hence at first, we evaluated the cytotoxicity of MgO NPs against normal human lung fibroblast CCD-25Lu cells and several types of cancerous cells such as HeLa cells, SNU-16 and AGS cell lines by the MTT assay method. The cytotoxicity results of MgO NPs against cancer cells are displayed in Fig. 4. No obvious toxicity of MgO NPs against normal fibroblast cells was observed even at higher concentrations of MgO (300 $\mu\text{g ml}^{-1}$) as shown in Fig. 4(a). It was evident from Fig. 4(b)–(d) that the cancerous cells were more sensitive to MgO NPs. The figure shows both dose dependent and time dependent toxicity of MgO NPs towards cancer cells. These results suggest that MgO can effectively kill the cancer cells in a dose dependent manner in 24 h, and only a little difference in toxicity was observed for 72 h.

Moreover, significant toxicity was observed in cancerous cells at higher concentrations of MgO NPs (200 and 300 $\mu\text{g ml}^{-1}$). This is supported by the experimental result of Ge *et al.* in which MgO shows toxicity at only higher concentrations.²⁰ The IC_{50} values of MgO NPs against HeLa cells, SNU-16 and AGS cell types were found to be 174.0, 240.03 and 223.33 $\mu\text{g ml}^{-1}$ after 72 h exposure. Herein, the AGS cells were preferentially selected to evaluate the in-depth mechanism of the MgO induced toxicity since gastric cancer remains the second most common cause of death from cancer worldwide and in many Asian countries. Especially in Korea, gastric cancer ranks as the most common cancer among men.⁴⁹ The AGS cells treated with various concentrations of the MgO NPs were examined by fluorescence microscopy after Hoechst 33342 staining to characterize the MgO-induced apoptosis and study the structural changes occurring in the morphology. In general, morphological changes, such as cell

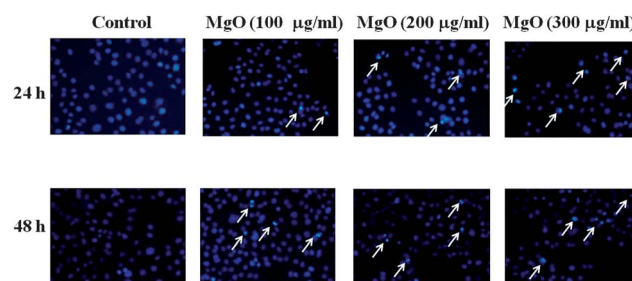


Fig. 5 MgO nanoparticle-induced apoptosis in AGS cells (magnification 300 \times). Morphological changes in AGS cells after MgO exposure for 24 and 48 h, respectively. Cells were stained with Hoechst 33342. Arrows indicate cells with condensed and fragmented chromatin, and apoptotic bodies.

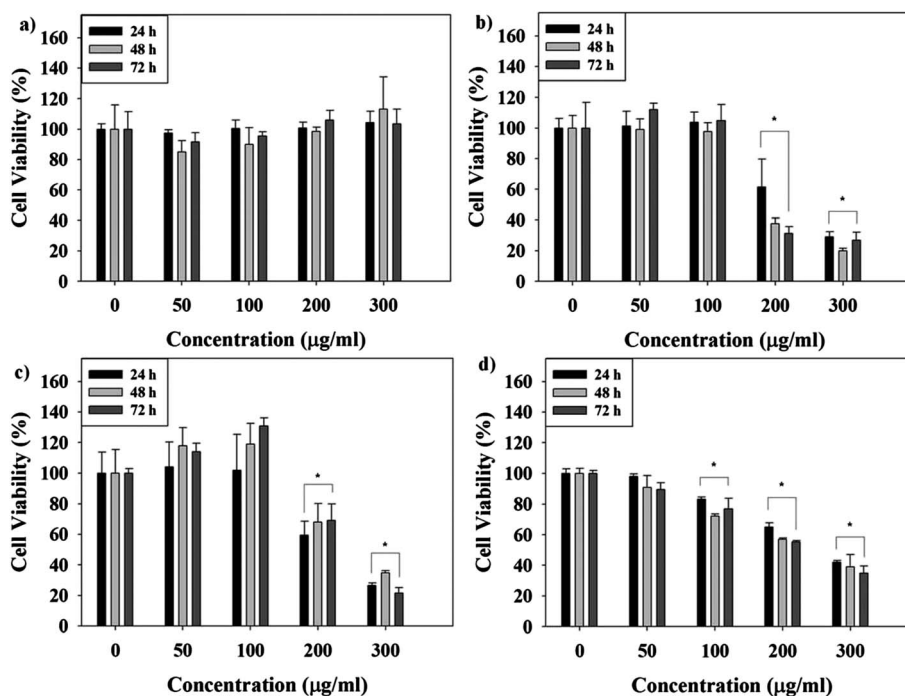


Fig. 4 Cytotoxicity of MgO nanoparticles against (a) normal human lung fibroblast CCD-25Lu cells, (b) HeLa cells, (c) SNU-16 cells and (d) AGS cell lines treated for 24, 48 and 72 h respectively. Untreated cells were used as controls. Cell viability without treatment was taken as 100%.

shrinkage and condensed and fragmented chromatin, are associated with apoptotic cell death.²⁹ Fig. 5 shows the Hoechst 33342 staining results obtained using fluorescence microscopy. As seen in Fig. 5, control cells did not show any apoptotic bodies. Nuclear staining with Hoechst 33342, a fluorescent DNA-binding dye, revealed fragmented and condensed nuclei in the nanoparticle-treated cells, which is typical of apoptotic phenomena (Fig. 5). The cells treated with increasing concentrations of MgO NPs showed a progressive accumulation of the condensed and fragmented chromatin and the apoptotic bodies (arrows) in a dose and time dependent manner. This illustrates the apoptosis mechanism of cell death occurring in cancerous cells after exposure to MgO NPs.

Western blotting of apoptosis-related proteins suggested that MgO NPs induced apoptosis in AGS cells as shown in Fig. 6. Dose dependent decrease in the level of Caspase 3, and subsequent increase in its cleaved form along with increase in the level of cleaved PARP strongly indicated that MgO induced apoptosis in AGS cells in a concentration dependent manner. Furthermore, the decrease in the anti-apoptotic protein Bcl-2 also pointed in favor of apoptosis caused by MgO in AGS cells in a dose dependent manner. FACS analysis was carried out to further confirm whether the MgO NPs-induced apoptosis in AGS cells is due to ROS generation. Herein, 300 $\mu\text{g ml}^{-1}$ MgO NPs-treated AGS cell lines were loaded with H₂DCFDA and their ROS

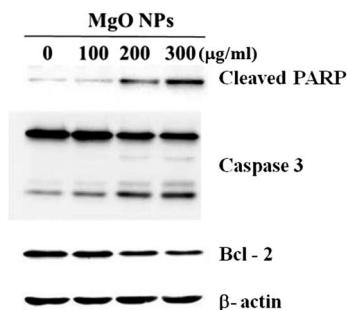


Fig. 6 Immunoblot analysis of apoptosis-related protein expression in MgO-treated AGS cells. Cells were lysed after 72 h of incubation with the indicated concentration of MgO NPs. Cellular proteins were separated by SDS-PAGE and transferred onto PVDF membranes. The membranes were probed with the indicated primary antibodies, then with secondary antibodies. β -actin was used as an internal control.

status was subsequently analyzed by flow cytometry for 6 h. H₂DCFDA is a reduced form of fluorescein, which can be converted into its fluorescent form with the cleavage of acetate groups by the intracellular esterases and oxidation. It is evident from Fig. 7 that ROS levels are higher in the cells treated with MgO NPs as compared with those in the control group.

The most debated mechanism of nanoparticle toxicity towards biological systems is their ability to stimulate the generation of reactive oxygen species (ROS), which leads to cell death due to oxidative stress.^{50,51} Previous reports showed that ZnO, TiO₂, and Ag nanoparticles are able to destroy the biological systems by the oxidative stress mechanism due to ROS generation.^{13,14,52,53} In order to determine the effect of ROS generation or the free radical modulation activity of MgO NPs, the lipid peroxidation assay experiment was performed.⁵⁴ MgO NPs enhanced the ultrasound-induced lipid peroxidation. In comparison with the control group, lipid peroxidation was increased by 117, 132 and 159% after exposure to 25, 50 and 100 $\mu\text{g ml}^{-1}$ of MgO ($p < 0.05$), respectively. This was consistent with the experimental results of Sun *et al.* in which MgO showed a dose dependent ROS generation.²² The mechanism of the formation of ROS on the surface of MgO NPs is still unclear. There are many reports on the formation of ROS, such as superoxide anions and hydrogen peroxide radicals, on the surface of MgO nanoparticles.^{18,19,55} Few reports suggested the presence of defect states/surface oxygen anions on the surface of MgO NPs resulting in the formation of ROS due to surface characteristics.^{34,56} UV-vis spectra of MgO NPs, as shown in Fig. 2(a), show the presence of four and three co-ordinated surface anions in the edges and corners and Fig. 3(b) shows the emission due to oxygen vacancies correspondingly, which are considered to be chemically reactive sites⁵⁷ that might be responsible for the generation of ROS on the surfaces. This is in agreement with the previous report on the electron spin resonance spectroscopy (ESR) study of MgO showing the generation of O₂⁻ radicals on the MgO surface.⁵⁸ However, further studies are needed to investigate more about the detailed physics underlying the reactions occurring at the oxide surface states resulting in ROS generation. It is well known that both superoxide anions and hydrogen peroxide are highly reactive oxygen species, which can create oxidative stress in the cellular system.⁵⁹ When the generated ROS overwhelms the levels of the cellular antioxidant defense system, it results in a state of oxidative stress,

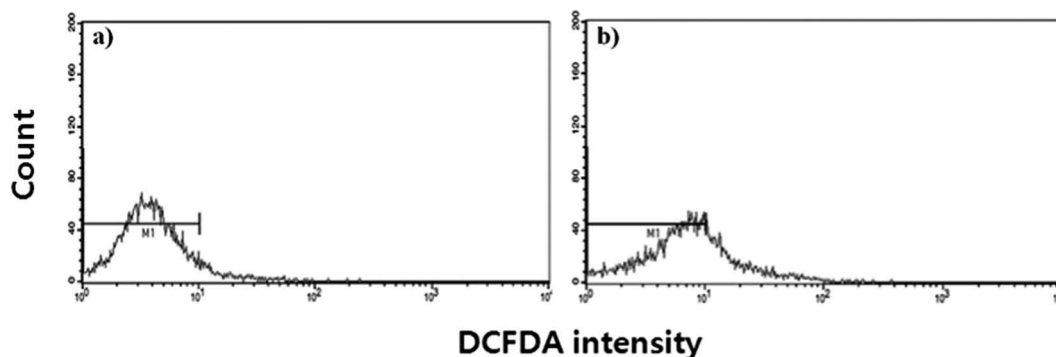


Fig. 7 ROS was increased by MgO nanoparticles in AGS cells. Cells were incubated with 300 $\mu\text{g ml}^{-1}$ of MgO nanoparticles for (a) 0 h and (b) 6 h and then cells were stained with H₂DCFDA, scraped, washed and analyzed by flow cytometric analysis.

thereby leading to cell death.^{60,61} The interaction between MgO NPs and cancer cells is also important in the toxicity mechanism. Since the MgO surface possesses a basic nature which can result in low surface energy⁶² under the acidic environment of the cancer cells, it can strongly interact with the cancer cells leading to apoptosis through elevated ROS levels. A similar mechanism was also proposed by Sasidharan *et al.* in their study which showed that ZnO nanocrystals in the acidic cancer microenvironment resulted in oxidative stress due to elevated ROS stress, mitochondrial superoxide formation, and depolarization of the mitochondrial membrane, leading to apoptosis.⁶³ In our case, MgO NPs enhanced the lipid peroxidation that evidences the involvement of ROS generation which is further confirmed by flow cytometric analysis, as shown in Fig. 7, proving the ROS mediated damage in AGS cell lines due to MgO NPs exposure. Furthermore, Fig. 6 clearly evidences the cell death due to apoptosis in AGS cell lines and morphological changes in the AGS cells are also observed by Hoechst 33342 staining experiments as shown in Fig. 5. Altogether, these results indicated a primary mechanism of MgO nanoparticles toxicity against cancer cells by the generation of ROS that results in the induction of apoptosis.

In summary, our findings demonstrate the mechanism of the toxicity of MgO NPs towards cancerous cells. The cytotoxicity results show both dose and time dependent toxicity of MgO NPs toward cancer cells. MgO NPs enhanced ultrasound induced lipid peroxidation suggesting the active role of ROS in the toxicity mechanism. The western blot analysis together with the flow cytometry analysis of cells treated with MgO NPs confirmed the apoptotic pathway of cell death due to elevated ROS levels. In addition to their use as MRI contrast agents, and in hyperthermia and nano-cryosurgery in the treatment of cancer, our findings extended the potential utility of MgO NPs in nanomedicine for cancer therapy as a novel alternative to chemotherapy due to their toxicity towards cancer cells through apoptosis by ROS generation.

Acknowledgements

This research was supported by a National Research Foundation of Korea (NRF) Grant under contract numbers 2011-0015829 and 2010-0012641.

References

- 1 S. Prakash, M. Malhotra, W. Shao, C.-T. Duchesneau and S. Abbasi, *Adv. Drug Delivery Rev.*, 2011, **63**, 1340.
- 2 H. Kim, J.-Y. Moon, A. Mosaddik and S.-K. Cho, *Food Chem. Toxicol.*, 2010, **48**, 2435.
- 3 J. Huang, H. Li, W. Chen, G.-H. Lv, X.-Q. Wang, G.-P. Zhang, K. Ostrikov, P.-Y. Wang and S.-Z. Yang, *Appl. Phys. Lett.*, 2011, **99**(1-3), 253701.
- 4 K. Karthikeyan, A. Babu, S.-J. Kim, R. Murugesan and K. Jeyasubramanian, *Cancer Nanotechnol.*, 2011, **2**, 95.
- 5 J. L. Arias, L. H. Reddy and P. Couvreur, *J. Mater. Chem.*, 2012, **22**, 7622.
- 6 N. K. Singh, S. K. Singh, D. Dash, B. P. Purkayastha, J. K. Roy and P. Maiti, *J. Mater. Chem.*, 2012, **22**, 17853, Advance article.
- 7 M. Premanathan, K. Karthikeyan, K. Jeyasubramanian and G. Manivannan, *Nanomedicine: Nanotechnology, Biology and Medicine*, 2011, **7**, 184.
- 8 P. Sanpui, A. Chattopadhyay and S.-S. Ghosh, *ACS Appl. Mater. Interfaces*, 2011, **3**, 218.
- 9 C. R. Patra, R. Bhattacharya and P. Mukherjee, *J. Mater. Chem.*, 2010, **20**, 547.
- 10 K.-M. Reddy, K. Feris, J. Bell, D.-G. Wingett, C. Hanley and A. Punnoose, *Appl. Phys. Lett.*, 2007, **90**(1-3), 213902.
- 11 A. Niu, Y. Han, J. Wu, N. Yu and Q. Xu, *J. Phys. Chem. C*, 2010, **114**, 12728.
- 12 W. Zhou, X. Liu and J. Ji, *J. Mater. Chem.*, 2012, **22**, 13969.
- 13 M. Ahamed, M. J. Akhtar, M. Raja, I. Ahmad, M. K. Siddiqui, M. S. AlSalhi and S. A. Alrokayan, *Nanomedicine*, 2011, **7**, 904.
- 14 P. Thevenot, J. Cho, D. Wavhal, R. B. Timmons and L. Tang, *Nanomedicine*, 2008, **4**, 226.
- 15 H. Ding, K.-T. Yong, I. Roy, H. E. Pudavar, W. C. Law, E. J. Bergey and P. N. Prasad, *J. Phys. Chem. C*, 2007, **111**, 12552.
- 16 L. Bertinetti, C. Drouet, C. Combes, C. Rey, A. Tampieri, S. Coluccia and G. Martra, *Langmuir*, 2009, **25**, 5647.
- 17 P. K. Stoimenov, R. L. Klinger, G. L. Marchin and K. J. Klabunde, *Langmuir*, 2002, **18**, 6679.
- 18 S. Makhluף, R. Dror, Y. Nitzan, Y. Abramovich, R. Jelinek and A. Gedanken, *Adv. Funct. Mater.*, 2005, **15**, 1708.
- 19 K. Krishnamoorthy, G. Manivannan, S.-J. Kim, K. Jeyasubramanian and M. Premanathan, *J. Nanopart. Res.*, 2012, **14**, 1063.
- 20 S. Ge, G. Wang, Y. Shen, Q. Zhang, D. Jia, H. Wang, Q. Dong and T. Yin, *IET Nanobiotechnol.*, 2011, **5**, 36.
- 21 J. Sun, S. Wang, D. Zhao, F. H. Hun, L. Weng and H. Liu, *Cell Biol. Toxicol.*, 2011, **27**, 333.
- 22 J. C. K. Lai, M. B. Lai, S. Jandhyam, V. V. Dukhande, A. Bhushan, C. K. Daniels and S. W. Leung, *Int. J. Nanomed.*, 2008, **3**, 533.
- 23 C. M. Boubeta, L. Balcells, R. Cristofol, C. Sanfeliu, E. Rodríguez, R. Weissleder, S. L. Piedrafitra, K. Simeonidis, M. Angelakeris, F. Sandiumenge, A. Calleja, L. Casas, C. Monty and B. Martínez, *Nanomedicine: Nanotechnology, Biology and Medicine*, 2010, **6**, 362.
- 24 A. Chalkidou, K. Simeonidis, M. Angelakeris, T. Samaras, C. M. Boubeta, Ll. Balcells, K. Papazisis, C. D. Samara and O. J. Kalogirou, *J. Magn. Magn. Mater.*, 2011, **323**, 775.
- 25 Z. Q. Lei, L. Li, G. J. Li, C. W. Leung, J. Shi, C. M. Wong, K. C. Lo, W. K. Chan, C. S. K. Mak, S. B. Chan, N. M. M. Chan, C. H. Leung, P. T. Lai and P. W. T. Pong, *J. Appl. Phys.*, 2012, **111**, 07E505.
- 26 D.-R. Di, Z.-Z. He, Z.-Q. Sun and J. Liu, *Nanomedicine: Nanotechnology, Biology and Medicine*, 2012, 1-9, DOI: 10.1016/j.nano.2012.02.010, in press.
- 27 K. Karthikeyan, N. Poornaprakash, N. Selvakumar and K. Jeyasubramanian, *J. Nanostruct. Polym. Nanocompos.*, 2009, **5**, 83-88.
- 28 J. Carmichael, W. G. Degraff, A. F. Gazdar, J. D. Minna and J. B. Mitchell, *Cancer Res.*, 1987, **47**, 936.
- 29 T.-T. Mai, J.-Y. Moon, Y.-W. Song, P.-Q. Viet, P.-V. Phuc, J.-M. Lee, T.-H. Yi, M. Cho and S.-K. Cho, *Cancer Lett.*, 2012, **321**, 144.
- 30 I. Parrilla, J. M. Vazquez, C. Cuello, M. A. Gil, J. Roca, D. D. Berardino and E. A. Martinez, *Reproduction*, 2004, **128**, 615.
- 31 J.-Y. Moon, A. Mosaddik, H. Kim, M. Cho, H.-K. Choi, Y. S. Kim and S.-K. Cho, *Food Chem.*, 2011, **125**, 369.
- 32 K. Krishnamoorthy, S. Natarajan, S.-J. Kim and J. Kadarkaraithangam, *Mater. Express*, 2011, **1**, 329.
- 33 P. Ouraipryvan, T. Sreethawong and S. Chavadej, *Mater. Lett.*, 2009, **63**, 1862.
- 34 M. Sterrer, O. Diwald and E. Knozinger, *J. Phys. Chem. B*, 2000, **104**, 3601.
- 35 L. Kumari, W. Z. Li, C.-H. Vannoy, R.-M. Leblanc and D.-Z. Wang, *Ceram. Interfaces*, 2009, **35**, 3355.
- 36 T. Berger, M. Sterrer, S. Stankic, J. Bernardi, O. Diwald and E. Knozinger, *Mater. Sci. Eng., A*, 2005, **25**, 664.
- 37 M. Rezaei, M. Khajenoori and B. Nematollahi, *Powder Technol.*, 2011, **205**, 112.
- 38 H. S. Kim and H. W. Kim, *Acta Phys. Pol., A*, 2009, **116**, 58.
- 39 K. Ishikawa, N. Fujima and H. Komura, *J. Appl. Phys.*, 1985, **57**, 973.
- 40 G. Pacchioni, *ChemPhysChem*, 2003, **4**, 1041.
- 41 S. Xie, X. Han, Q. Kuang, Y. Zhao, Z. Xie and L. Zheng, *J. Mater. Chem.*, 2011, **21**, 7263.
- 42 B. M. Maoz, E. Tirosh, M. B. Sadan, I. Popov, Y. Rosenberg and G. Markovich, *J. Mater. Chem.*, 2011, **21**, 9532.
- 43 Y. Hao, G. Meng, C. Ye, X. Zhang and L. Zhang, *J. Phys. Chem. B*, 2005, **109**, 11204.
- 44 C. Fang, N. Bhattarai, C. Sun and M. Zhang, *Small*, 2009, **5**, 1637.

- 45 V. Sharma, D. Anderson and A. Dhawan, *Apoptosis*, 2012, **17**, 852.
- 46 M. Ahamed, M. J. Akhtar, M. Raja, I. Ahmad, M. K. J. Siddiqui, M. S. AlSalhi and S. A. Alrokayan, *Nanomedicine*, 2011, **7**, 904.
- 47 V. Sharma, R. K. Shukla, N. Saxena, D. Parmar, M. Das and A. Dhawan, *Toxicol. Lett.*, 2009, **185**, 211.
- 48 M. Ahamed, R. Posgai, T. J. Gorey, M. Nielsen, S. M. Hussain and J. J. Rowe, *Toxicol. Appl. Pharmacol.*, 2010, **242**, 263.
- 49 J.-L. Ku, K.-H. Kim, J.-S. Choi, S.-H. Kim, Y.-K. Shin, H. J. Chang, J.-M. Bae, Y. W. Kim, J. H. Lee, H.-K. Yang, W.-H. Kim, S.-Y. Jeong and J.-G. Park, *Cell. Oncol.*, 2010, **35**, 127.
- 50 G. Applerot, A. Lipovsky, R. Dror, N. Perkas, Y. Nitzan, R. Lubart and A. Gedanken, *Adv. Funct. Mater.*, 2009, **19**, 842.
- 51 M. Veerapandian and K. Yun, *Appl. Microbiol. Biotechnol.*, 2011, **90**, 1655.
- 52 Z. Hu, Y. Huang, S. Sun, W. Guan, Y. Yao, P. Tang and C. Li, *Carbon*, 2012, **50**, 994.
- 53 M.-I. Sriram, S.-B. Manikant, K. Kalishwaralal and S. Gurunathan, *Int. J. Nanomed.*, 2010, **5**, 753.
- 54 A.-K. Jana, S. Agarwal and S.-N. Chatterjee, *Radiat. Res.*, 1990, **124**, 7.
- 55 J. Sawai, H. Kojima, H. Igarashi, A. Hashimoto, S. Shoji, T. Sawaki, A. Hakoda, E. Kawada, T. Kokugan and M. Shimizu, *World J. Microbiol. Biotechnol.*, 2000, **16**, 187.
- 56 M. Sterrer, T. Berger, O. Diwald and E. Knozinger, *J. Am. Chem. Soc.*, 2003, **125**, 195.
- 57 S. Stankic, M. Muller, O. Diwald, M. Sterrer, E. Knozinger and J. Bernardi, *Angew. Chem., Int. Ed.*, 2005, **44**, 4917.
- 58 O. Diwald, M. Sterrer, E. Knozinger, P.-V. Sushko and A.-L. Shluger, *J. Chem. Phys.*, 2002, **116**, 1707.
- 59 S. S. K. Wijeratne, S.-L. Cuppett and V. Schlegel, *J. Agric. Food Chem.*, 2005, **53**, 8768.
- 60 T. Xia, M. Kovoichich, J. Brant, M. Hotze, J. Sempf, T. Oberley, C. Sioutas, J.-I. Yeh, M.-R. Wiesner and A. E. Nel, *Nano Lett.*, 2006, **6**, 1794.
- 61 K. Krishnamoorthy, M. Veerapandian, L.-H. Zhang, K. S. Yun and S.-J. Kim, *J. Phys. Chem. C.*, 2012, **116**, 17280.
- 62 P. Thissen, V. Thissen, S. Wippermann, Y. J. Chabal, G. Grundmeier and W. G. Schmidt, *Surf. Sci.*, 2012, **606**, 902.
- 63 A. Sasidharan, P. Chandran, D. Menon, S. Raman, S. Nair and M. Koyakutty, *Nanoscale*, 2011, **3**, 3657.